A genome-edited β-cell model of Prader-Willi syndrome reveals chronic deficits in endoplasmic reticulum chaperones and insulin secretion

Erik A. Koppes[1], Marie A. Johnson[1], James J. Moresco[2,#], Patrizia Luppi[3], Dale W. Lewis[4], Donna B. Stolz[3], Jolene K. Diedrich[2], John R. Yates III[2], Ronald C. Wek[5], Simon C. Watkins[3], Susanne M. Gollin[4], Hyun J. Park[4], Peter Drain[3], Robert D. Nicholls[1]

[1] Division of Genetic and Genomic Medicine, Department of Pediatrics, UPMC Children's Hospital of Pittsburgh, Pittsburgh, PA 15224; [2] Department of Molecular Medicine and Neurobiology, The Scripps Research Institute, La Jolla, CA 92037; [3] Department of Cell Biology, University of Pittsburgh School of Medicine, Pittsburgh, PA 15261; [4] Department of Human Genetics, University of Pittsburgh School of Public Health, Pittsburgh, PA 15261; [5] Department of Biochemistry and Molecular Biology, Indiana University School of Medicine, Indianapolis, IN 46202

Address correspondence to R.D.N.:
Dr. Robert D. Nicholls, Department of Pediatrics, UPMC Children's Hospital of Pittsburgh, Rangos Research Building, 4401 Penn Avenue, Pittsburgh, PA 15224; robert.nicholls@chp.edu; Tel., 1-412-692-7855; Fax, 1-412-692-7816.

[#] Current address: Center for Genetics of Host Defense, UT Southwestern Medical Center, Dallas, TX

Keywords: CRISPR/Cas9; genomic imprinting; hormone secretion; metabolic disease; pancreatic islet

ABSTRACT

Prader-Willi syndrome (PWS) is a multisystem disorder caused by loss of expression of a cluster of paternally-expressed, imprinted genes. Neonatal failure to thrive is followed by childhood-onset hyperphagia, obesity, neurobehavioral abnormalities, and hormonal deficits. Prior evidence from a mouse model with a deletion of the orthologous PWS-gene domain identified abnormal pancreatic islet development with deficient insulin secretion, hypoglucagonemia, and postnatal onset of progressive, lethal hypoglycemia. To investigate the role of PWS-genes in β-cell secretory function, we used CRISPR/Cas9 genome-editing to generate isogenic, clonal INS-1 insulinoma lines with 3.16 Mb deletions of the silent, maternal (control) or active, paternal (PWS) alleles. PWS β-cells showed a significant reduction in basal and glucose-stimulated insulin secretion, signifying a deficiency in cell-autonomous insulin secretion. Parallel proteome and transcriptome studies revealed reduced levels of secreted peptides and twelve endoplasmic reticulum (ER) chaperones, including HSPA5 and HSP90B1. In contrast to the dosage compensation previously seen for ER chaperones in *Hspa5* or *Hsp90b1* gene knockouts, compensation is precluded by the widespread deficiency of ER chaperones in PWS β-cells. Consistent with the reduced ER chaperone levels, PWS INS-1 β-cells are more sensitive to ER stress, leading to earlier activation of all three arms of the unfolded protein response. These results suggest that a chronic deficit of ER chaperones in PWS β-cells leads to a delay in ER transit and/or folding of insulin and other cargo along the secretory pathway. The findings illuminate the pathophysiological basis of hormone deficits in PWS and implicate PWS-imprinted genes in β-cell secretory pathway function.

INTRODUCTION

Prader-Willi syndrome (PWS) is a multisystem disorder caused by loss of expression of a large contiguous cluster of paternally-expressed, imprinted genes from human chromosome 15q11.2 (1-3). Clinically, PWS is characterized by failure to thrive (FTT) with hypotonia, developmental and cognitive delay, behavioral problems, short stature, hypogonadism, hyperphagia, and early-onset obesity (3, 4). Prominent endocrine features of PWS include deficiencies of multiple hormones, including growth hormone (GH), oxytocin, gonadotropins, insulin-like growth factor (IGF-I), thyroid hormones, amylin (IAPP), and pancreatic polypeptide (PP) (1, 4-9). In addition, plasma insulin is lower than expected in PWS relative to the degree of obesity (10, 11). Episodes of hypoglycemia have been reported in PWS patients, suggesting an imbalance in glucose homeostasis (12, 13). In contrast, plasma ghrelin is grossly elevated in PWS (3, 10, 14). Although the PWS literature suggests a hypothalamic etiology (3), the mechanisms for endocrine and metabolic dysfunction in PWS have not been elucidated.

Our earlier studies of a transgenic-PWS (TgPWS) mouse model harboring a deletion of the orthologous PWS-imprinted domain demonstrated severe FTT, abnormalities in fetal pancreatic islet development and architecture, reduced α- and β-cell mass, increased apoptosis, and postnatal onset of progressive hypoglycemia that led to lethality within the first postnatal week (15, 16). Plasma insulin and glucagon levels were low during fetal and neonatal life (15, 16), with significantly reduced basal and glucose-induced insulin secretion from cultured TgPWS islets and a delay in secretion of an insulin-Timer fluorescent protein biomarker from β-cells *in vivo* (16). These results suggested that PWS-imprinted genes are required for the development and secretory function of pancreatic endocrine cells.

The PWS-imprinted domain is comprised of ten paternally-expressed imprinted genes conserved in human and rodents (with an additional two genes each unique to human and rodents), encoding lncRNAs, snoRNAs, miRNAs, or distinct proteins (1, 2, 17-22). These imprinted genes are predominantly expressed in neuronal (18, 20, 23) and neuroendocrine lineages (22), as well as pancreatic endocrine cells (α-, β-, δ-, and PP cells, with only low expression in acinar, ductal, or undefined cells) based on recent gene-specific (16) and single cell RNA sequencing (scRNA-seq) studies (24-26). Further, *SNRPN* has decreased islet expression in β-cell failure due to saturated fatty acids (27) or cytokines (28), while *SNORD116* and *SNORD107* occur in islet exosomes and decrease by IL-1β and IFN-γ treatment (29). Finally, *SNORD116* RNA levels are greatly reduced in MODY3 β-cells (30). These observations suggest that PWS-gene products function in the endocrine pancreas and especially in β-cells.

To assess the role of PWS genes in pancreatic β-cell secretory pathway function, we used CRISPR/Cas9 genome editing within the INS-1(832/13) insulinoma (β)-cell line (31) to generate 3.16 Mb deletions of the complete PWS-domain.. Following validation of a cell-autonomous insulin secretion deficit in the PWS INS-1 model, we performed molecular profiling by proteomic and transcriptomic approaches. The results revealed deficits in multiple secreted hormones as well as in critical endoplasmic reticulum (ER) chaperones that are components of secretory protein folding and trafficking pathways (32-37), identifying a novel gene regulatory network (GRN) and providing mechanistic insight into PWS-gene function in pancreatic β-cells.

RESULTS

Generation of INS-1 cell lines with PWS-gene deletions: To investigate the functions of PWS-genes in β-cell secretory function, we used CRISPR/Cas9 genome-editing to target 3.16 Mb deletions encompassing the PWS-genes (**Fig. 1A**; **Fig. S1A**) in rat INS-1(832/13)::mCherry insulinoma cells (hereafter termed INS-1) that secrete rat and human insulin (31) and express a mouse *Ins2* C-peptide-mCherry biosensor (38) in insulin secretory granules (Geng X, Luppi P, Nicholls RD, Drain P: manuscript in preparation). The large deletions were visualized in about 9% of unselected, transfected cells as determined by fluorescence *in situ* hybridization (FISH) (**Fig. S1B**). INS-1 lines with PWS-domain deletions were derived through sequential targeting and clonal isolation of cell lines initially harboring deletions of the silent maternal allele, followed by targeting of the remaining paternal loci, culminating in the creation of homozygous PWS-deletion lines (**Fig. 1B**). This process first led to isolation of two lines with a PWS-region deletion (5-5, 5-9) identified by deletion-breakpoint PCR (**Fig. 1C**) and DNA sequencing (**Fig. S2A,B**), and confirmed by FISH using BAC probes from within and outside the PWS-domain (**Fig. S1C-F**). One PWS allele was deleted in all interphase and metaphase cells of line 5-5 (**Fig. S1D**), indicating clonal isolation of a cell line with a PWS-domain deletion. Initially, line 5-9 was more complex, as FISH showed two cell types with either no deletion (most cells) or a PWS-domain deletion (**Fig. S1E**); additionally, similar proportions of cells lacked mCherry fluorescence, likely due to epigenetic silencing (as DNA analysis indicated the transgene was present) or were mCherry-positive, respectively. This allowed separation by fluorescence-activated cell sorting (FACS), with establishment of a clonal mCherry-positive cell line (5-9) harboring a PWS-domain deletion (**Fig. S1F**).

Clonal engineered cell lines 5-5 and 5-9 were inferred to have maternal-deletions of the rat PWS-domain as evidenced by **1)** detection of only an unmethylated allele at the PWS-imprinting center (PWS-IC) by bisulfite PCR whereas parental INS-1 and control lines had biparental DNA methylation (**Fig. 1D**); and **2)** expression of 10 PWS-imprinted loci by reverse-transcription-PCR (RT-PCR) (**Fig. S1G**; and data not shown), indicating the presence of an active, paternal-allele (**Fig. S1H**). Finally, the presence of mutations at sgRNA target sites on the intact, paternal chromosome, termed scarred mutation alleles, identified a single nucleotide insertion at the sgRNA1 site (**Fig. S1I**; **Fig. S2C-E**) but different nucleotide insertions at the sgRNA3 site (**Fig. S1I**; **Fig. S2F-H**), the latter indicating an independent origin for the cell lines, 5-5 and 5-9.

To specifically target the paternal allele of lines 5-5 and 5-9, we used rat-specific sgRNA sets internal to the first targeting sites to generate slightly smaller 3.143 Mb PWS-deletions (**Fig. S3A-C**). The use of FISH demonstrated that about 5% of unselected, transfected cells had a PWS-deletion (**Fig. S3D**). We chose maternal deletion (control) line 5-9 for a second round of transfections and clonal isolation, generating control lines 2 and 16 (**Fig. 1B,E**; **Fig. S3E,F**) as well as PWS lines 19 and 25, with an expected paternal deletion-PCR product and PWS line 3 with a larger than expected deletion-PCR product (**Fig. 1B,E**; **Fig. S3G**). DNA sequencing confirmed PWS-deletion breakpoints for lines 19 and 25 (**Fig. S4A-C**) as well as for line 3, although the latter arose from a larger deletion at an alternate (alt) proximal alt-sgRNA70-3 targeting site with a DNA repair event that inserted a fragment of *E. coli* DNA in the breakpoint junction (**Fig. S4D**). FISH studies confirmed that lines 3 and 25 had deletions of the PWS-domain on each allele (**Fig. S3H,I**); however, FISH analysis also revealed that line 25 was mosaic for cells with diploid or tetraploid PWS-signals (**Fig. S3I**). Consequently, line 25 was not used further. In

contrast, line 19 had a residual fraction of cells (1-3.7%) with an intact paternal allele as shown by FISH (**Fig. S3J**) and droplet digital PCR (ddPCR) (**Fig. S5**) which was removed by cell dilution and isolation of five clonal lines 19-1 through 19-5 (**Fig. 1B**; **Fig. S3K,L**; **Fig. S7A**). Finally, sgRNA target sites not deleted or involved in a deletion breakpoint were assessed for scarred mutation alleles identifying a 28-nt deletion at alt-sgRNA70-3 in PWS lines 19-1 and 19-4 (**Fig. S3N**; **Fig. S4E-L**).

Genomic copy number was confirmed by ddPCR (**Fig. 1F**; **Fig. S5**; **Fig. S6**), establishing a set of three control lines (5-9, 2, 16) with hemizygosity for maternal-allele deletions (**Fig. S1H**) and three PWS INS-1 lines (3, 19-1, 19-4) with homozygosity for PWS-domain deletions (**Fig. S3M**). An absence of PWS-gene expression in all PWS lines was shown by RT-PCR for each PWS-imprinted gene (**Fig. 1G**; **Fig. S7A,B**) and by western blot analysis for the SmN polypeptide encoded by *Snrpn* (**Fig. 1H**). Intriguingly, PWS INS-1 lines showed a very low level of apparent expression of the PWS-imprinted gene *Snurf* by RT-PCR (**Fig. S7A**; **Fig. S8A,B**). Sequencing of the RT-PCR products identified an expressed *ψSnurf* sequence within a recently evolved *ψSnurf-ψSnrpn* locus located in an intron of the *Mon2* gene (**Fig. S8B,C**). Using a *Pml*I variant between *Snurf* and *ψSnurf* (**Fig. S8D**), we confirmed expression specifically of *ψSnurf* with complete silencing of *Snurf* (**Fig. S8B**), as expected for PWS INS-1 lines. Scattered mutations in the *ψSnurf* (**Fig. S8D**) and *ψSnrpn* (**Fig. S8E,F**) segments likely inactivate any coding potential (**Fig. S8G**; **Fig. S8H**). In summation, these results establish a panel of clonal INS-1 lines homozygous for ~ 3.16 Mb deletions, also termed PWS β-cell lines, and similarly, of clonal control lines with a deletion only involving the silent, maternal allele.

PWS INS-1 cell lines show deficits in insulin secretion and ER chaperones: To determine whether PWS INS-1 cell lines have secretory deficits, we carried out insulin secretion assays under low (2.2 mM) and high (22 mM) glucose conditions. The three PWS cell lines displayed a striking deficit in both basal and glucose-induced insulin secretion as compared to the isogenic control INS-1 lines (**Fig. 2**). However, both the PWS and control cell lines had a similar increase from each basal level for glucose-stimulated insulin secretion (**Fig. 2**), indicating that PWS β-cells were not deficient in glucose responsiveness.

Next, mass spectrometry was used to assess changes in the cellular proteome and all secreted peptides in PWS *vs.* control INS-1 cell lines, under insulin secretion conditions of 22 mM glucose, separating cellular proteins by methanol-acetic acid extraction into small and large protein fractions with the latter analyzed by quantitative proteomics (**Fig. S9A**). Unexpectedly, in PWS INS-1 cells there was a striking deficiency of multiple endoplasmic reticulum (ER) chaperone proteins, including GRP78/BiP (HSPA5), GRP94/endoplasmin (HSP90B1), PDIA4, HYOU1, CRELD2, and DNAJB11, with lesser albeit significant reductions in SDF2L1, DNAJC3, PDIA6, and PDIA3, and a modest decrease in PPIB (**Fig. 3**). Similar deficits of residual amounts of many of these ER chaperones as well as MANF were detected in the small protein fraction (**Fig. S9B**). Furthermore, in PWS β-cell lines there was reduced abundance of numerous hormones co-secreted from INS-1 cells, including rat insulin-1 and insulin-2, mouse insulin-2, and human insulin (pre-pro-, pro-, C-peptide, and mature versions of each), as well as reductions in processed and precursor forms of IAPP and NPY, detected in both the cellular small protein fraction (**Fig. S9B**) and residual amounts in the large protein fraction

by quantitative proteomics (**Fig. 3**). In contrast, the full-length secretory granule protein, chromogranin B (CHGB), and the C-terminal CHGB (CCB)-peptide were increased 2-fold (**Fig. 3**; **Fig. S9B**). Extending both the insulin secretion data (**Fig. 2**) and the cellular protein deficiencies (**Fig. 3**; **Fig. S9B**), mass spectrometry analysis of peptides secreted into the culture media demonstrated reduced levels of all forms of insulins and IAPP in PWS β-cells compared to control (**Fig. S9C**). There was also a reduction in secreted levels of the 14 amino acid WE14 peptide processed from chromogranin A (CHGA), but no changes in the CHGA precursor and processed forms in either secreted or cellular fractions. Secreted levels of chromogranin B were increased in PWS (**Fig. S9C**), further illustrating the concordance between cellular and secreted peptide levels in PWS *vs.* control INS-1 lines. These results indicate that deletion of PWS-genes sharply lowers secretion of insulin and other peptide hormones (IAPP, NPY, CHGA-WE14) and this reduction is associated with deficiencies in many ER chaperones.

Reduced mRNA levels for hormones and ER chaperones in PWS INS-1 cell lines: Many of the PWS-imprinted genes (**Fig. 1A**) are suggested to function in gene expression (17, 18, 20, 21, 39, 40). To gain insight into the molecular basis for insulin secretion and ER chaperone deficits in PWS INS-1 lines, high-throughput total RNA sequencing (RNA-seq) was used to identify differentially expressed genes (DEGs) (**Fig. 4A-C**; **Tables S1,S2**). Visualization by a heatmap clustergram (**Fig. 4A**) indicates that PWS clonal lines and control clonal lines each grouped together with similar expression profiles. A volcano plot depicting the magnitude, direction, and statistical significance of DEGs in the 3 PWS *vs.* 3 control lines illustrates no appreciable expression (Log2 Fold Change < -5) of PWS-

imprinted genes with remaining DEGs symmetrically orientated around the ordinate axis with a near equivalent number of significantly upregulated (105) and downregulated (123) genes (**Fig. 4B**). The PWS transcripts with complete loss of expression specifically in PWS INS-1 lines include *Snurf*, *Snrpn*, *Ipw*, *Mkrn3*, all four snoRNAs (*Snord116, Snord115, Snord107* and Snord*109*), miRNA (*Mir344* isoforms), and duplicated U1-*Snurf* sequences (**Fig. 4B**), as also seen by RT-PCR (**Fig. 1G**; **Fig. S7A,B**; **Fig. S8A,B**). Three PWS-imprinted genes, *Ndn*, *Magel2*, and *Frat3* (*Peg12*), were not detected as DEGs as these are not expressed in any of parental, control, or PWS INS-1 lines (see GSE190334), confirmed also by RT-PCR (data not shown). These loci are present by genomic PCR, suggesting an epigenetic inactivation in the INS-1 founder cell line, although silencing is not widespread, as *Mkrn3* and *Mir-344* are interspersed with the silenced loci (see **Fig. 1A**) and are well-expressed in control INS-1 lines (**Fig. S7B**; **Fig. S10**).

To ensure complete coverage of the INS-1 transcriptome, RNA-seq of small stable RNAs in the PWS *vs.* control cell lines was carried out, culminating in the identification of 58 significant differentially expressed miRNAs and snoRNAs (**Fig. S10A,B**; **Table S3**). Congruent with the RNA-seq data, all but three correspond to PWS-imprinted small RNAs, including duplicated *MiR-344*, *Snord116* and *Snord115* loci, as well as single copy *Snord107* and *Snord64* loci (**Fig. S10A,B**). In addition, *Mir135b*, *Mir3065*, and *Mir212* were downregulated in PWS INS-1 lines (**Fig. S10B**), although predicted targets were not DEGs by RNA-seq. Eleven of the top 25 highly expressed miRNAs in the rat INS-1 β-cell model (**Table S4**), including *Mir375*, *Mir148a*, *Mir183*, *Mir30d*, *Mir27b*, *Mir25*, *Mir26a2*, *Mir26a*, *Mir192*, *Mir125a*, and *Mir141* are also in the top 25 expressed miRNAs for a human β-cell model (41). Within INS-1 cells, expression of PWS-region *Snord116* copies

make up 13.8% of the top 188 highly expressed snoRNAs and cumulatively would be the thirteenth highest expressed, with *Snord64* also in and *Snord107* just outside the top 100 (**Table S5**), although snoRNAs are poorly studied as a small RNA class.

In addition to the loss of PWS-imprinted gene expression in the PWS INS-1 lines, four additional classes of DEGs were identified by manual annotation analysis of RNA-seq data (**Fig. 4B**). These DEG classes encoded: **1)** hormones (e.g., *Iapp*, *Npy*, *mIns2::mCherry*) that were significantly reduced; **2)** nine ER chaperones that were lowered including *Sdf2l1*, *Hspa5*, *Creld2*, *Dnajb11*, *Hyou1*, *Pdia4*, *Dnajc2*, *Hsp90b1*, and *Pdia6*; **3)** "neuronal active zone" proteins that had increased expression, including *Cacna1a*, *Rph3al*, *Bsn*, *Rimbp2*, *Cacna1d*, *Pclo*, and *Chgb* (most that are known to play a role in insulin exocytosis) (42-47); and **4)** two related transmembrane proteins involved in vesicle acidification (*Tmem176a,b*) (48) whose expression were also enhanced. Gene ontology and pathway analysis of downregulated genes (excluding PWS-imprinted genes) through Enrichr or DAVID highlighted enrichment of multiple ER functional groups including those in ER protein processing, and the unfolded protein response (UPR) that are linked with both IRE1 and ATF6 (**Fig. 4C**; **Fig. S11A-C**). Finally, based on the input of downregulated DEGs, Enrichr predicted potential upstream transcriptional regulatory factors, including NFYA/NFYB (a cofactor of ATF6α, hereafter ATF6), CPEB1, RFX5, IRF3, CREB1, SREBF1, XBP1, and PPARB/D (**Fig. S12**).

Transcriptional changes observed by RNA-seq were corroborated by RT-droplet digital PCR (RT-ddPCR) analyses using RNA from independent biological replicates of each PWS and control INS-1 line (**Fig. 4D-H**; **Fig. S13**; **Fig. S14**). We validated equal expression of the housekeeping gene, *Gapdh*, and loss of expression of *Snord116* (**Fig. 4D**), as well as significant down-regulation in PWS INS-1 lines of 10 genes encoding ER

chaperones (**Fig. 4E**: *Hspa5*, *Hsp90b1*, *Pdia4*, *Pdia6*, *Ppib*, *Creld2*, *Sdf2l1*, *Dnajb11*, *Dnajc3*, and *Hyou1*), of endogenous hormones (**Fig. 4F**: *Npy*, *Iapp*), and of the mouse *Ins2-mCherry* transgene (**Fig. 4G**). Further, another eight downregulated genes in PWS β-cells were verified (**Fig. S14**) including *Syt1*, encoding a Ca^{2+}-sensor (49) and *Jph3*, encoding a junctophilin involved in ER-plasma membrane contact bridges (50); each with roles in insulin secretion (49, 50); *Derl3*, involved in ER-associated degradation (ERAD) (51), *Mylip*, encoding an E3 ubiquitin ligase regulating the LDL receptor (52), *Atp10a*, encoding a lipid flippase (53), and *Tap1* and *Tap2*, encoding ER antigenic peptide transporters that play a role in type 1 diabetes (54). Additionally, up-regulation of four genes was confirmed by RT-ddPCR (**Fig. 4H**), including *Cacna1a*, *Chgb*, *Tmem176a*, and *Tmem176b*.

Several other observations merit note. In contrast to the proteomics data wherein all endogenous forms of insulin were decreased in PWS INS-1 lines, neither rat *Ins1* nor *Ins2* mRNA levels were statistically different between PWS and control lines in the RNA-seq or RT-ddPCR (**Fig. 4F**) expression profiling. Only a minority of DEGs identified by RNA-seq did not validate by RT-ddPCR, including several encoding neuronal active zone proteins (**Fig. S14**), possibly arising from cell culture media differences between biological replicates. Additionally, an apparent increase in expression of the human *INS-neoR* transgene in PWS lines (**Fig. 4G**) was an artifactual consequence of epigenetic silencing of the transgene, specifically in control line 16 (**Fig. S13A,I-K,M**). Interestingly, although both mRNA (*Pcsk1*) and protein levels of prohormone convertase PC1 were reduced in iPSC-derived neurons from PWS patients and in whole islets of inbred *Snord116*-deficient mice (22, 55), neither PC1 protein (not shown) nor *Pcsk1* mRNA levels were changed in PWS INS-1 cell lines (**Fig. 4F**). Finally, no markers of activation of apoptotic or other cell

death pathways were observed by RNA-seq or proteomics, consistent with the absence of any increase in cell death observed in cultured PWS or control INS-1 cells (data not shown). Indeed, electron microscopy showed normal mitochondria, rough ER, and other subcellular structures in PWS and control INS-1 lines (**Fig. S15**). The difference in observations *in vivo* where increased apoptosis was observed in a subset of α- and β-cells in TgPWS fetal islets (16) and *in vitro* (this study) may reflect the use of enriched culture medium with reduced cellular stress under cell culture conditions. In summary, the transcriptome studies show that loss of PWS-gene expression in PWS β-cell lines is accompanied by widespread alterations in mRNA levels most notably encoding secreted peptides and ER chaperones.

Confirmation of insulin and ER chaperone protein deficits in PWS INS-1 lines: To further address the predicted disruptions of the ER and secretory pathway, we used western blot analyses to measure cellular levels of insulin and ER chaperones in control and PWS INS-1 lines. Levels of numerous forms of insulin polypeptides detected by an anti-insulin antibody were each significantly decreased in PWS INS-1 lines compared to controls, including diminished amounts of pro-insulin, pre-pro-insulin, and pro-mInsulin-2::mCherry bands (**Fig. 5A,D**). Additionally, using an anti-mCherry antibody, we observed that PWS cells have significantly lower levels of the proinsulin form of the mouse insulin2-mCherry transgene with a trend towards reduction in the processed C-peptide form (**Fig. 5B,E**). Importantly, use of a KDEL antibody to identify proteins with the ER retention motif confirmed significant deficiencies in levels of the two major ER chaperone proteins, GRP78/BiP and GRP94, in PWS INS-1 cell lines (**Fig. 5C,F**). These results indicate that

there are major disruptions of the protein folding machinery and attendant reductions in insulin processing and secretion in the PWS INS-1 cells.

PWS INS-1 cells are more sensitive to activation by ER stressors: Chaperones, such as GRP78 and GRP94, not only have essential roles in protein folding and protein trafficking in the ER but disruptions of these chaperone functions are reported to sensitize cells to agents that stress this organelle (56-61). Therefore, we assessed whether the PWS INS-1 lines and their reduced levels of ER chaperones (**Fig. 3-5**) would accentuate activation of the three sensory proteins of the UPR. First, ER stress activates IRE1α to catalyze mRNA processing of the *Xbp1* mRNA to generate the functional XBP1 transcription factor (61); this non-canonical "splicing" of *Xbp1* transcripts occurs at low and equal levels in PWS and control INS-1 cells under DMSO control growth conditions but is enhanced by treatment with thapsigargin to initiate ER stress (**Fig. 6A,D**; **Fig. S16A,B**). Importantly, production of "spliced" *Xbp1* mRNA in thapsigargin-treated cells occurs significantly more robustly at earlier 2 h and 3 h timepoints for PWS than for control INS-1 lines (**Fig. 6A,D**; **Fig. S16A,B**) but normalizes by 4-5 h (**Fig. S16A,B**). These results suggest that while the magnitude of IRE1 activation is greater in the PWS INS-1 cells, the duration is comparable. Second, phosphorylation of eIF2α by PERK (60) was assessed, with PWS INS-1 lines showing significantly higher levels of eIF2α pSer51 phosphorylation than control lines when ER stress was induced by 5 h of thapsigargin treatment (**Fig. 6B,E**). Phosphorylated eIF2α inhibits general translation but preferentially translates certain stress adaptive genes, including ATF4 and CHOP; transcripts of these genes were unaffected in unstressed PWS INS-1 cells as measured by RNA-seq.

Third, dissociation of ER-retained ATF6 from GRP78 by ER stressors such as de-glycosylation agents (57, 58) enable it to move to the Golgi, where it is processed to an activated nuclear (N) form, ATF6-N, which regulates expression of genes encoding many ER chaperones, including GRP78 and others. In PWS and control INS-1 cells, ER stress induced by tunicamycin, as expected, de-glycosylates full-length glycosylated (FL-G) ATF6 of ~ 102-kD to an unglycosylated 90-kD (FL-UG) form and the processed ATF6-N form of 55-kD (**Fig. 6C**; **Fig. S17A**). The loss of the ATF6 FL-G form by deglycosylation occurs at the same rate for PWS and control cell lines (**Fig. S17B**). However, the ratio of the processed ATF6-N (due to higher production in PWS than control INS-1 cells) to full-length unglycosylated 90-kD (with a higher level in control than PWS INS-1 cells) is significantly greater for PWS compared to control INS-1 cells at 2-5 h timepoints (**Fig. 6C,F**; also see **Fig. S17A,B**). Thus, ATF6 is being activated to ATF6-N earlier and more robustly in PWS than in control INS-1 β-cell lines. Combined, these results on ER stress activation of the IRE1α/XBP1, PERK/eIF2α, and ATF6-N pathways indicate that PWS INS-1 β-cells are more sensitive than control INS-1 β-cells to ER stressors.

DISCUSSION

Although PWS has long been assumed to be a neuroendocrine disease of the hypothalamus (3, 22), prior studies using mouse models implicated a role for the pancreatic endocrine system (16, 55). Here, we generated a novel PWS INS-1 β-cell model system through deletion of the ~3.16 Mb PWS-orthologous imprinted domain in which to investigate PWS β-cell biology. A significant reduction in both basal and glucose-stimulated insulin secretion was observed in PWS INS-1 β-cells, recapitulating the insulin secretory deficit observed in PWS mice (16), and demonstrating that it is a cell autonomous rather than a systemic deficit. Further, by implementing proteomic and transcriptomic approaches, we identified diminished levels of secreted proteins (insulins, amylin, Npy) and ER chaperone proteins in PWS β-cells, including the two most abundant chaperones (GRP78 and GRP94), as well as other cellular components that are essential for protein folding and proinsulin trafficking. These observations point to the crucial roles of PWS-genes in pancreatic β-cells, including regulatory control of hormone synthesis and secretion and of the homeostatic control of ER chaperone biosynthesis.

A critical observation is that a PWS-imprinted gene or genes are involved in coordinately regulating numerous ER chaperones and hormones secreted from the β-cell, such that the absence of PWS genes leads to a chronic reduction in expression of a multitude of ER chaperones at the mRNA and protein levels as well as for secreted hormone expression (insulin, amylin, Npy). Physiologically, this is the opposite of the ER stress response, in which ER chaperones are coordinately upregulated by ER stress (59-61). Prior evidence from mouse knockout models of key ER chaperone genes has shown that these are subject to dosage compensation to maintain homeostasis. Although

knockouts for either *Grp78* or *Grp94* are lethal early in mouse embryogenesis, heterozygous mice are viable (32, 62-64). Intriguingly, upregulation of GRP94 and other ER chaperones occurs in *Grp78* +/- mice (62) and similarly for GRP78 in *Grp94* +/- mice (63), indicative of dosage compensation among ER chaperones. A similar mechanism operates in *Grp78* +/- mice to attenuate diet-induced obesity and insulin resistance (64). Compensatory changes with upregulation of GRP94 or GRP78 (BiP) and other ER chaperones including PDIA6 also occurred with shRNA knockdown of *Grp78* or *Grp94*, respectively, in a mouse cell line (65). In contrast, the widespread deficiency of ER chaperones, including GRP78 and GRP94, that we describe for PWS INS-1 β-cells would preclude compensatory increases. Because of an inability to compensate, we hypothesize that PWS β-cells have a chronic deficit in production of ER chaperones which would interfere with folding of proinsulin and/or delay ER transit of cargo (e.g., hormones) along the secretory pathway. Consistent with this hypothesis, our previous *in vivo* results using a Timer fluorescent protein biomarker demonstrated an accumulation of aged insulin in islets of PWS mice (16). Importantly, a chronic ER chaperone deficiency in β-cells with reduced hormone secretion in PWS implies a physiologically distinct state from the acute β-cell deficits that occur in type 2 diabetes (T2D) (35-37).

Insulin secretion is abnormal both *in vivo* in the PWS-deletion mouse model (16) and the new PWS INS-1 β-cell model. In the latter, all insulins expressed and secreted from INS-1 cells are decreased, as measured by proteomics and western blot analyses. Despite decreased mRNA expression of a *mIns2::mCherry* transgene and for numerous genes encoding ER chaperones, there is no change in mRNA expression for the endogenous *Ins2* and *Ins1* genes. This suggests that not only do PWS-genes act through transcriptional regulation of target genes in the ER chaperone regulatory pathway, but

that translational mechanisms for insulin mRNAs may be affected in PWS β-cells. Subsequent to translation of the insulin precursor, folding of insulin or trafficking through the ER is also affected in PWS β-cells due to the downregulated ER chaperones GRP94 and GRP78. Indeed, these ER chaperones have known functions in insulin secretion. GRP94 directly binds pro-insulin, and chemical inhibition or genetic ablation results in diminished insulin processing, retained immature granules, and activation of the PERK ER stress pathway (66). Intriguingly, GRP94 levels are upregulated in β-cells from T2D patients, likely as a compensatory mechanism to enhance insulin production (66). Similarly, knockdown of *Grp78* levels in INS-1 832/13 cells reduced insulin biosynthesis and secretion (67) and GRP78 levels are also increased in T2D (68). Furthermore, overexpression of GRP78 in β-cells protects against obesity-induced T2D in mice (69).

In addition to essential roles in protein folding and protein trafficking out of the ER, ER chaperones are also sensors of ER stress, a physiological quality control mechanism responding to accumulation or failure in degradation of misfolded or unfolded secretory proteins (3, 56, 59, 70, 71). ER stress responses are governed by three major pathways, regulated by IRE1α/XBP1, PERK/eIF2α/Ddit3(CHOP), and ATF6, that aim to recover ER homeostasis in part by upregulating ER chaperone gene expression, although failure in recovery can lead to cell death (36, 56, 59). Perhaps due to the β-cell demand for folding of high levels of insulin, a protein notoriously difficult to fold (71), β-cells maintain a basal level of ATF6 activation sufficient to uniquely maintain a higher level of GRP78 than for most cell types (72). In unstressed cells, GRP78/BiP forms stable complexes in the ER lumen (56, 57) with each of IRE1α, PERK, and ATF6 (PERK is also bound by GRP94). ER stress releases GRP78/BiP and induction of each pathway. Indeed, our results establish that reduced levels of ER chaperones do affect activation of all three ER stress

pathways in PWS β-cells treated with thapsigargin or tunicamycin. Therefore, PWS β-cells have a basal metabolic state that is more sensitive to ER stressors and poised to a greater degree for response by all three master regulatory pathways, which we suggest arises from a burden of chronic ER chaperone deficiency that decreases the threshold required for ER-stress activation. As the ATF6 and XBP1 pathways lead to upregulated transcription of many genes encoding ER chaperones (73-76), this might represent an attempt to normalize ER chaperone function, but also may create an opportunity for a therapeutic window by which mild ER stressors for PWS cells could temporarily activate ER chaperone expression, leading to improved ER homeostasis.

The coordinate downregulation of at least ten ER chaperone genes, including *Hspa5* and *Hsp90b1*, in PWS β-cells supports the hypothesis that a PWS-imprinted gene or genes regulates a transcription factor(s) (TF) that coordinately regulates ER chaperones in a GRN. Although many of the DEGs that encode ER chaperones in PWS INS-1 β-cells are known ATF6 and/or XBP1 targets (73-76), numerous ATF6, IRE1α/XBP1, and ATF4/CHOP (PERK pathway) target genes (73-80) are not dysregulated in PWS INS-1 lines, suggesting that novel GRN pathways are downstream of PWS genes. Initial candidate TFs within the PWS-ER chaperone GRN are those with binding site motifs enriched in the promoters of DEGs in PWS β-cells, including, but not limited to the known ATF6 co-factor NFYA, which has roles in insulin secretion and glucose homeostasis (81), as well as PPARB/D also with known roles in β-cell mass and insulin secretion (82). Which PWS gene or genes regulates the PWS→TF→ER chaperone network? Neither *Magel2* nor *Ndn* have a role, as they are not expressed in INS-1 cells, while top candidates highly expressed in INS-1 cells are *Snrpn*, encoding the SmN spliceosomal protein (39), *Snurf*, encoding a small arginine-rich nuclear protein (17),

and *Snord116*, a tandemly duplicated snoRNA that may function as a sno-lncRNA acting as a molecular “sink” for FOX2 and other RNA binding proteins in alternative splicing pathways (21, 83), although *SNORD116* may also regulate direct RNA targets through canonical box C/D snoRNA interactions. Further studies are necessary to distinguish amongst the candidate PWS genes and to identify downstream GRN steps leading to coordinated ER chaperone expression.

Recent work has shown hypothalamic deficiencies in *Magel2*-deficient mice as well as for iPSC- and dental-pulp stem cell neuronal models, specifically in secretory granule components including PCSK1, PCSK2, CPE, granins (e.g., CHGB and others), and numerous neuropeptides (22). These studies established that MAGEL2 plays a role in hypothalamic neuroendocrine cells by regulating neuropeptide production and secretion via endosome recycling to prevent lysosomal degradation of secretory granule proteins (22), which is downstream of the ER in protein trafficking and secretory pathways. As discussed above, our study shows that another PWS-gene (e.g., *Snrpn*, *Snurf*, and/or *Snord116*) is putatively responsible for regulating ER chaperone and hormone (e.g., insulin) biosynthesis and secretion from pancreatic β-cells. In contrast to the reported reduction of prohormone convertase PC1 in PWS iPSC-derived neurons and in *Snord116*-null mice (55), no deficiency in *Pcsk1* mRNA or PC1/3 levels or in *Pcsk2* or PC2 was observed in PWS β-cell lines, which may reflect differences in cell type, genetics, or experimental conditions. Combined, these observations in hypothalamic neuroendocrine cells and pancreatic β-cells indicate that at least two PWS-imprinted genes regulate related neuropeptide and peptide hormone secretory pathways, suggesting that the PWS domain may function as a “mammalian operon” or

synexpression group (84, 85). As the PWS-domain arose evolutionarily in a eutherian mammalian ancestor (86), this suggests emergence of functions acting as molecular rheostats to regulate protein secretion pathways in endocrine cells that control growth, metabolism, and neural pathways.

Maintaining glucose homeostasis relies on exquisite coordination between secretion of the opposing hormones insulin and glucagon from pancreatic β- and α-cells, respectively, in response to changes in blood glucose; disruption of these processes contributes to the pathogenesis of metabolic disorders, including T2D (36, 87-90). Although insulin and glucagon play opposite regulatory roles both in normal metabolic homeostasis and dysfunction in T2D, PWS mice are remarkable in having low blood levels of both insulin and glucagon (15, 16). As recent studies indicate that GRP78 interacts with glucagon in α-cells (91), it will be important to further assess dysregulation of ER chaperones and glucagon secretion in PWS α-cells both in cell culture and within PWS mouse models. Intriguingly, quantitative trait locus (QTL) studies in mice link genetic variation in blood insulin and glucose levels in or near to the PWS-orthologous domain (92). Further studies are warranted to examine the role of PWS-imprinted genes in T2D-related traits in humans, and whether β-cell or other endocrine cell deficits in ER chaperones and hormone secretion contribute to clinical phenotypes, including episodes of hypoglycemia in PWS subjects (12, 13). As PWS genes regulate islet development, β- and α-cell secretion (15, 16), and a GRN affecting ER chaperone and insulin secretion (as shown in this study), identifying mechanisms by which PWS-genes carry out these critical β-cell functions will illuminate the pathogenesis and may reveal effective treatments for not only PWS, but for common disorders, such as T2D, with deficits in glycemic homeostasis and islet hormone secretory pathways.

MATERIALS AND METHODS

Materials and methods are provided in *SI Appendix, Materials and Methods*. These include materials and methods for cell culture, genome editing, molecular cytogenetics, droplet digital PCR (ddPCR) genomic copy number assays, DNA methylation, insulin secretion assays, reverse transcription-PCR, RT-droplet digital-PCR assays, proteomics, immunoblot analyses, transmission electron microscopy, RNA-seq and bioinformatics, sections that include **Tables S6-S9** and all statistical methods.

DATA AVAILABILITY

The RNA-seq FASTQ files and processed data associated from this study have been deposited in the NCBI Gene Expression Omnibus (GEO) under SuperSeries GSE190337 including GSE190334 (total RNA-seq) and GSE190336 (small RNA-seq), assigned to BioProject PRJNA786769.

The TMT quantitative proteomics data files have been deposited at ProteomeXchange under accession number PXD#.

ACKNOWLEDGEMENTS

We thank Dr. Michael R. Rickels and Heather W. Collins at the Penn Diabetes Center RIA/Biomarkers Core, Mary F. Sanchirico for the protein database, and Drs. Rebecca A. Simmons and Dwi Kemaladewi for review of the manuscript. This project used the University of Pittsburgh Health Sciences Sequencing Core at UPMC Children's Hospital of Pittsburgh, for RNA sequencing. This work was supported by a research grant to R.D.N. from the Foundation for Prader-Willi Research (FPWR) and funding to R.D.N. from the Storr Family Foundation through the Prader-Willi Syndrome Association

(PWSA). J.J.M., J.K.D., and J.R.Y. were supported by the National Institute of General Medical Sciences (8P41 GM103533). This manuscript is dedicated to PWS families and especially the Storr family for their support of our PWS research program.

AUTHOR CONTRIBUTIONS

EAK, MAJ, JJM, PL, DWL, DBS, JKD performed experiments and analyzed data; EAK performed bioinformatics analyses; EAK, JJM, DBS, JRY, SCW, SMG, HJP, PD, RDN designed experiments and interpreted data; RCW provided a critical reagent; EAK, RDN wrote the manuscript; all co-authors reviewed and approved manuscript drafts and final version.

REFERENCES

1. R. A. Costa, I. R. Ferreira, H. A. Cintra, L. H. F. Gomes, L. D. C. Guida, Genotype-phenotype relationships and endocrine findings in Prader-Willi syndrome. *Front Endocrinol* **10**, 864 (2019).
2. M. S. Chung, M. Langouet, S. J. Chamberlain, G. G. Carmichael, Prader-Willi syndrome: reflections on seminal studies and future therapies. *Open Biol* **10**, 200195 (2020).
3. M. Tauber, C. Hoybye, Endocrine disorders in Prader-Willi syndrome: a model to understand and treat hypothalamic dysfunction. *Lancet Diabetes Endocrinol* **9**, 235-246 (2021).
4. G. Muscogiuri *et al.*, Prader- Willi syndrome: An uptodate on endocrine and metabolic complications. *Rev Endocr Metab Disord* **20**, 239-250 (2019).
5. T. Tomita, G. Greeley, Jr., L. Watt, V. Doull, R. Chance, Protein meal-stimulated pancreatic polypeptide secretion in Prader-Willi syndrome of adults. *Pancreas* **4**, 395-400 (1989).
6. H. J. Lee *et al.*, Delayed response of amylin levels after an oral glucose challenge in children with Prader-Willi syndrome. *Yonsei Med J* **52**, 257-262 (2011).
7. C. L. Deal *et al.*, Growth Hormone Research Society workshop summary: consensus guidelines for recombinant human growth hormone therapy in Prader-Willi syndrome. *J Clin Endocrinol Metab* **98**, E1072-1087 (2013).
8. M. D. Fountain, Jr., C. P. Schaaf, MAGEL2 and oxytocin-implications in Prader-Willi syndrome and beyond. *Biol Psychiatry* **78**, 78-80 (2015).
9. H. J. Hirsch, T. Eldar-Geva, F. Bennaroch, Y. Pollak, V. Gross-Tsur, Sexual dichotomy of gonadal function in Prader-Willi syndrome from early infancy through the fourth decade. *Hum Reprod* **30**, 2587-2596 (2015).
10. A. P. Goldstone *et al.*, Fasting and postprandial hyperghrelinemia in Prader-Willi syndrome is partially explained by hypoinsulinemia, and is not due to peptide YY3-36 deficiency or seen in hypothalamic obesity due to craniopharyngioma. *J Clin Endocrinol Metab* **90**, 2681-2690 (2005).
11. K. H. Paik *et al.*, Peptide YY, cholecystokinin, insulin and ghrelin response to meal did not change, but mean serum levels of insulin is reduced in children with Prader-Willi syndrome. *J Korean Med Sci* **22**, 436-441 (2007).
12. Y. Ma *et al.*, Nutritional and metabolic findings in patients with Prader-Willi syndrome diagnosed in early infancy. *J Pediatr Endocrinol Metab* **25**, 1103-1109 (2012).
13. R. A. Harrington, D. A. Weinstein, J. L. Miller, Hypoglycemia in Prader-Willi syndrome. *Am J Med Genet A* **164A**, 1127-1129 (2014).
14. D. E. Cummings *et al.*, Elevated plasma ghrelin levels in Prader Willi syndrome. *Nat Med* **8**, 643-644 (2002).
15. M. Stefan *et al.*, Hormonal and metabolic defects in a Prader-Willi syndrome mouse model with neonatal failure to thrive. *Endocrinology* **146**, 4377-4385 (2005).
16. M. Stefan *et al.*, Global deficits in development, function, and gene expression in the endocrine pancreas in a deletion mouse model of Prader-Willi syndrome. *Am J Physiol Endocrinol Metab* **300**, E909-922 (2011).
17. T. A. Gray, S. Saitoh, R. D. Nicholls, An imprinted, mammalian bicistronic transcript encodes two independent proteins. *Proc Natl Acad Sci U S A* **96**, 5616-5621 (1999).

18. J. Cavaille *et al.*, Identification of brain-specific and imprinted small nucleolar RNA genes exhibiting an unusual genomic organization. *Proc Natl Acad Sci U S A* **97**, 14311-14316 (2000).
19. R. D. Nicholls, J. L. Knepper, Genome organization, function, and imprinting in Prader-Willi and Angelman syndromes. *Annu Rev Genomics Hum Genet* **2**, 153-175 (2001).
20. S. Kishore, S. Stamm, The snoRNA HBII-52 regulates alternative splicing of the serotonin receptor 2C. *Science* **311**, 230-232 (2006).
21. H. Wu *et al.*, Unusual processing generates SPA lncRNAs that sequester multiple RNA binding proteins. *Mol Cell* **64**, 534-548 (2016).
22. H. Chen *et al.*, Loss of MAGEL2 in Prader-Willi syndrome leads to decreased secretory granule and neuropeptide production. *JCI Insight* **5** (2020).
23. J. C. Castle *et al.*, Digital genome-wide ncRNA expression, including snoRNAs, across 11 human tissues using polyA-neutral amplification. *PLoS One* **5**, e11779 (2010).
24. C. Benner *et al.*, The transcriptional landscape of mouse beta cells compared to human beta cells reveals notable species differences in long non-coding RNA and protein-coding gene expression. *BMC Genomics* **15**, 620 (2014).
25. J. Li *et al.*, Single-cell transcriptomes reveal characteristic features of human pancreatic islet cell types. *EMBO Rep* **17**, 178-187 (2016).
26. A. Segerstolpe *et al.*, Single-cell transcriptome profiling of human pancreatic islets in health and type 2 diabetes. *Cell Metab* **24**, 593-607 (2016).
27. M. Cnop *et al.*, RNA sequencing identifies dysregulation of the human pancreatic islet transcriptome by the saturated fatty acid palmitate. *Diabetes* **63**, 1978-1993 (2014).
28. D. L. Eizirik *et al.*, The human pancreatic islet transcriptome: expression of candidate genes for type 1 diabetes and the impact of pro-inflammatory cytokines. *PLoS Genet* **8**, e1002552 (2012).
29. P. Krishnan, F. Syed, N. Jiyun Kang, R. G. Mirmira, C. Evans-Molina, Profiling of RNAs from human islet-derived exosomes in a model of type 1 diabetes. *Int J Mol Sci* **20** (2019).
30. B. S. J. Low *et al.*, Decreased GLUT2 and glucose uptake contribute to insulin secretion defects in MODY3/HNF1A hiPSC-derived mutant beta cells. *Nat Commun* **12**, 3133 (2021).
31. H. E. Hohmeier *et al.*, Isolation of INS-1-derived cell lines with robust ATP-sensitive K+ channel-dependent and -independent glucose-stimulated insulin secretion. *Diabetes* **49**, 424-430 (2000).
32. G. Zhu, A. S. Lee, Role of the unfolded protein response, GRP78 and GRP94 in organ homeostasis. *J Cell Physiol* **230**, 1413-1420 (2015).
33. G. Rajpal, I. Schuiki, M. Liu, A. Volchuk, P. Arvan, Action of protein disulfide isomerase on proinsulin exit from endoplasmic reticulum of pancreatic beta-cells. *J Biol Chem* **287**, 43-47 (2012).
34. M. Sun, J. L. M. Kotler, S. Liu, T. O. Street, The endoplasmic reticulum (ER) chaperones BiP and Grp94 selectively associate when BiP is in the ADP conformation. *J Biol Chem* **294**, 6387-6396 (2019).
35. M. A. Kalwat, D. Scheuner, K. Rodrigues-Dos-Santos, D. L. Eizirik, M. H. Cobb, The pancreatic ß-cell response to secretory demands and adaption to stress. *Endocrinology* **162** (2021).
36. R. B. Sharma, H. V. Landa-Galvan, L. C. Alonso, Living dangerously: protective and harmful ER stress responses in pancreatic beta-cells. *Diabetes* **70**, 2431-2443 (2021).

37. J. Yong, J. D. Johnson, P. Arvan, J. Han, R. J. Kaufman, Therapeutic opportunities for pancreatic beta-cell ER stress in diabetes mellitus. *Nat Rev Endocrinol* **17**, 455-467 (2021).
38. S. Watkins *et al.*, Imaging secretory vesicles by fluorescent protein insertion in propeptide rather than mature secreted peptide. *Traffic* **3**, 461-471 (2002).
39. T. A. Gray *et al.*, Concerted regulation and molecular evolution of the duplicated SNRPB'/B and SNRPN loci. *Nucleic Acids Res* **27**, 4577-4584 (1999).
40. Q. Liu *et al.*, Neural-specific expression of miR-344-3p during mouse embryonic development. *J Mol Histol* **45**, 363-372 (2014).
41. N. Lawlor *et al.*, Multiomic profiling identifies cis-regulatory networks underlying human pancreatic beta cell identity and function. *Cell Rep* **26**, 788-801 e786 (2019).
42. K. Fujimoto *et al.*, Piccolo, a Ca2+ sensor in pancreatic beta-cells. Involvement of cAMP-GEFII.Rim2. Piccolo complex in cAMP-dependent exocytosis. *J Biol Chem* **277**, 50497-50502 (2002).
43. S. Obermuller *et al.*, Defective secretion of islet hormones in chromogranin-B deficient mice. *PLoS One* **5**, e8936 (2010).
44. M. C. Proverbio *et al.*, Whole genome SNP genotyping and exome sequencing reveal novel genetic variants and putative causative genes in congenital hyperinsulinism. *PLoS One* **8**, e68740 (2013).
45. T. M. Reinbothe *et al.*, The human L-type calcium channel Cav1.3 regulates insulin release and polymorphisms in CACNA1D associate with type 2 diabetes. *Diabetologia* **56**, 340-349 (2013).
46. F. Fan *et al.*, Exophilin-8 assembles secretory granules for exocytosis in the actin cortex via interaction with RIM-BP2 and myosin-VIIa. *Elife* **6** (2017).
47. K. Matsunaga, M. Taoka, T. Isobe, T. Izumi, Rab2a and Rab27a cooperatively regulate the transition from granule maturation to exocytosis through the dual effector Noc2. *J Cell Sci* **130**, 541-550 (2017).
48. L. Drujont *et al.*, RORgammat+ cells selectively express redundant cation channels linked to the Golgi apparatus. *Sci Rep* **6**, 23682 (2016).
49. N. Nakajima-Nagata *et al.*, Pdx-1 enables insulin secretion by regulating synaptotagmin 1 gene expression. *Biochem Biophys Res Commun* **318**, 631-635 (2004).
50. L. Li *et al.*, Junctophilin 3 expresses in pancreatic beta cells and is required for glucose-stimulated insulin secretion. *Cell Death Dis* **7**, e2275 (2016).
51. Y. Oda *et al.*, Derlin-2 and Derlin-3 are regulated by the mammalian unfolded protein response and are required for ER-associated degradation. *J Cell Biol* **172**, 383-393 (2006).
52. N. M. van Loon, D. Lindholm, N. Zelcer, The E3 ubiquitin ligase inducible degrader of the LDL receptor/myosin light chain interacting protein in health and disease. *Curr Opin Lipidol* **30**, 192-197 (2019).
53. T. Naito *et al.*, Phospholipid flippase ATP10A translocates phosphatidylcholine and is involved in plasma membrane dynamics. *J Biol Chem* **290**, 15004-15017 (2015).
54. D. Kronenberg-Versteeg *et al.*, Molecular pathways for immune recognition of preproinsulin signal peptide in type 1 diabetes. *Diabetes* **67**, 687-696 (2018).
55. L. C. Burnett *et al.*, Deficiency in prohormone convertase PC1 impairs prohormone processing in Prader-Willi syndrome. *J Clin Invest* **127**, 293-305 (2017).
56. A. Bertolotti, Y. Zhang, L. M. Hendershot, H. P. Harding, D. Ron, Dynamic interaction of BiP and ER stress transducers in the unfolded-protein response. *Nat Cell Biol* **2**, 326-332 (2000).

57. J. Shen, X. Chen, L. Hendershot, R. Prywes, ER stress regulation of ATF6 localization by dissociation of BiP/GRP78 binding and unmasking of Golgi localization signals. *Dev Cell* **3**, 99-111 (2002).
58. M. Hong *et al.*, Underglycosylation of ATF6 as a novel sensing mechanism for activation of the unfolded protein response. *J Biol Chem* **279**, 11354-11363 (2004).
59. I. Braakman, N. J. Bulleid, Protein folding and modification in the mammalian endoplasmic reticulum. *Annu Rev Biochem* **80**, 71-99 (2011).
60. B. F. Teske *et al.*, The eIF2 kinase PERK and the integrated stress response facilitate activation of ATF6 during endoplasmic reticulum stress. *Mol Biol Cell* **22**, 4390-4405 (2011).
61. Y. Tsuchiya *et al.*, IRE1-XBP1 pathway regulates oxidative proinsulin folding in pancreatic beta cells. *J Cell Biol* **217**, 1287-1301 (2018).
62. S. Luo, C. Mao, B. Lee, A. S. Lee, GRP78/BiP is required for cell proliferation and protecting the inner cell mass from apoptosis during early mouse embryonic development. *Mol Cell Biol* **26**, 5688-5697 (2006).
63. C. Mao *et al.*, Targeted mutation of the mouse Grp94 gene disrupts development and perturbs endoplasmic reticulum stress signaling. *PLoS One* **5**, e10852 (2010).
64. R. Ye *et al.*, Grp78 heterozygosity promotes adaptive unfolded protein response and attenuates diet-induced obesity and insulin resistance. *Diabetes* **59**, 6-16 (2010).
65. D. Eletto *et al.*, Limitation of individual folding resources in the ER leads to outcomes distinct from the unfolded protein response. *J Cell Sci* **125**, 4865-4875 (2012).
66. S. M. Ghiasi *et al.*, Endoplasmic reticulum chaperone glucose-regulated protein 94 is essential for proinsulin handling. *Diabetes* **68**, 747-760 (2019).
67. L. Zhang, E. Lai, T. Teodoro, A. Volchuk, GRP78, but not protein-disulfide isomerase, partially reverses hyperglycemia-induced inhibition of insulin synthesis and secretion in pancreatic β-Cells. *J Biol Chem* **284**, 5289-5298 (2009).
68. D. R. Laybutt *et al.*, Endoplasmic reticulum stress contributes to beta cell apoptosis in type 2 diabetes. *Diabetologia* **50**, 752-763 (2007).
69. T. Teodoro-Morrison, I. Schuiki, L. Zhang, D. D. Belsham, A. Volchuk, GRP78 overproduction in pancreatic beta cells protects against high-fat-diet-induced diabetes in mice. *Diabetologia* **56**, 1057-1067 (2013).
70. A. Tiwari *et al.*, SDF2L1 interacts with the ER-associated degradation machinery and retards the degradation of mutant proinsulin in pancreatic beta-cells. *J Cell Sci* **126**, 1962-1968 (2013).
71. J. Sun *et al.*, Proinsulin misfolding and endoplasmic reticulum stress during the development and progression of diabetes. *Mol Aspects Med* **42**, 105-118 (2015).
72. T. Teodoro, T. Odisho, E. Sidorova, A. Volchuk, Pancreatic beta-cells depend on basal expression of active ATF6alpha-p50 for cell survival even under nonstress conditions. *Am J Physiol Cell Physiol* **302**, C992-1003 (2012).
73. Y. Adachi *et al.*, ATF6 is a transcription factor specializing in the regulation of quality control proteins in the endoplasmic reticulum. *Cell Struct Funct* **33**, 75-89 (2008).
74. P. J. Belmont *et al.*, Coordination of growth and endoplasmic reticulum stress signaling by regulator of calcineurin 1 (RCAN1), a novel ATF6-inducible gene. *J Biol Chem* **283**, 14012-14021 (2008).
75. R. B. Sharma, C. Darko, L. C. Alonso, Intersection of the ATF6 and XBP1 ER stress pathways in mouse islet cells. *J Biol Chem* **295**, 14164-14177 (2020).

76. D. Acosta-Alvear *et al.*, XBP1 controls diverse cell type- and condition-specific transcriptional regulatory networks. *Mol Cell* **27**, 53-66 (2007).
77. B. Adamson *et al.*, A multiplexed single-cell CRISPR screening platform enables systematic dissection of the unfolded protein response. *Cell* **167**, 1867-1882 e1821 (2016).
78. L. Plate *et al.*, Small molecule proteostasis regulators that reprogram the ER to reduce extracellular protein aggregation. *Elife* **5** (2016).
79. T. J. Bergmann *et al.*, Chemical stresses fail to mimic the unfolded protein response resulting from luminal load with unfolded polypeptides. *J Biol Chem* **293**, 5600-5612 (2018).
80. S. M. Park, T. I. Kang, J. S. So, Roles of XBP1s in transcriptional regulation of target genes. *Biomedicines* **9** (2021).
81. Y. Liu *et al.*, Nuclear factor-Y in mouse pancreatic beta-cells plays a crucial role in glucose homeostasis by regulating beta-cell mass and insulin secretion. *Diabetes* **70**, 1703-1716 (2021).
82. J. Iglesias *et al.*, PPARbeta/delta affects pancreatic beta cell mass and insulin secretion in mice. *J Clin Invest* **122**, 4105-4117 (2012).
83. Q. F. Yin *et al.*, Long noncoding RNAs with snoRNA ends. *Mol Cell* **48**, 219-230 (2012).
84. C. Niehrs, N. Pollet, Synexpression groups in eukaryotes. *Nature* **402**, 483-487 (1999).
85. R. D. Nicholls, Incriminating gene suspects, Prader-Willi style. *Nat Genet* **23**, 132-134 (1999).
86. R. W. Rapkins *et al.*, Recent assembly of an imprinted domain from non-imprinted components. *PLoS Genet* **2**, e182 (2006).
87. P. Rorsman, M. Braun, Regulation of insulin secretion in human pancreatic islets. *Annu Rev Physiol* **75**, 155-179 (2013).
88. D. A. Sandoval, D. A. D'Alessio, Physiology of proglucagon peptides: role of glucagon and GLP-1 in health and disease. *Physiol Rev* **95**, 513-548 (2015).
89. P. V. Roder, B. Wu, Y. Liu, W. Han, Pancreatic regulation of glucose homeostasis. *Exp Mol Med* **48**, e219 (2016).
90. Y. C. Chen, A. J. Taylor, C. B. Verchere, Islet prohormone processing in health and disease. *Diabetes Obes Metab* **20 Suppl 2**, 64-76 (2018).
91. F. Asadi, S. Dhanvantari, Plasticity in the glucagon interactome reveals novel proteins that regulate glucagon secretion in alpha-TC1-6 cells. *Front Endocrinol* **9**, 792 (2018).
92. H. A. Lawson *et al.*, The importance of context to the genetic architecture of diabetes-related traits is revealed in a genome-wide scan of a LG/J x SM/J murine model. *Mamm Genome* **22**, 197-208 (2011).

FIGURES and FIGURE LEGENDS

Figure 1:

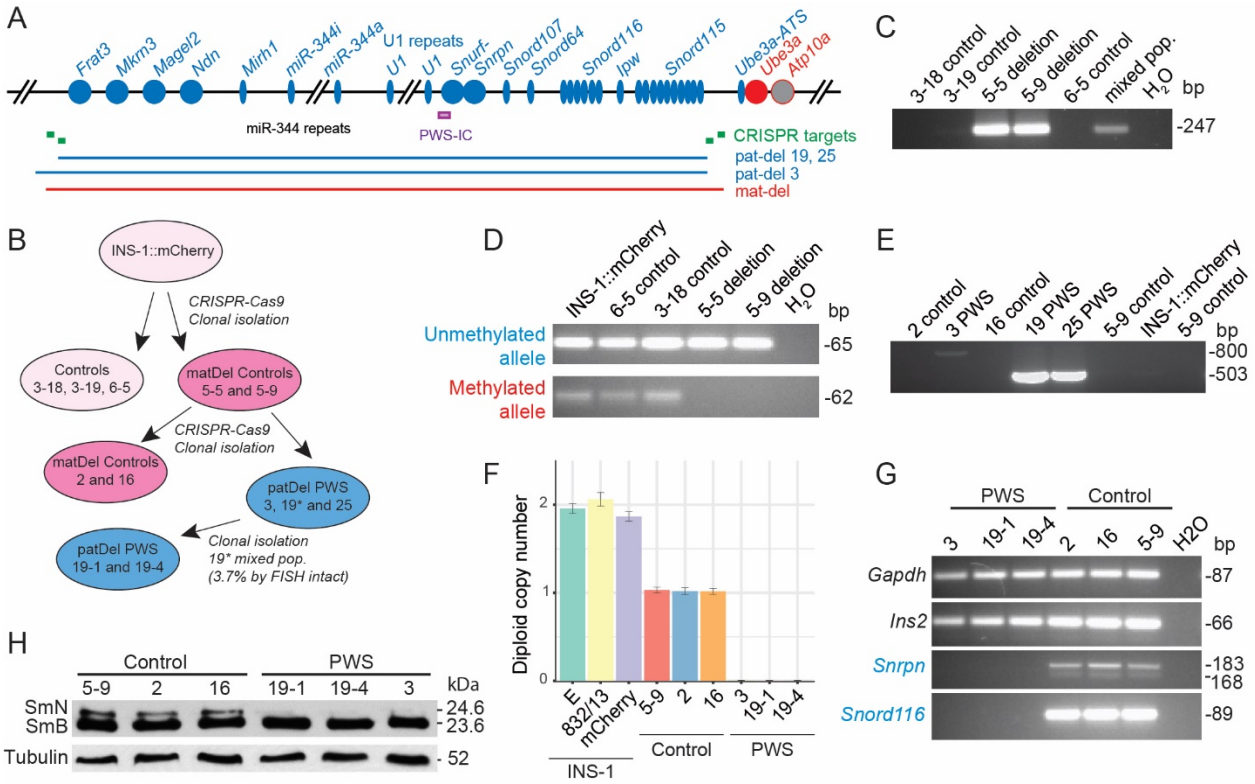

Figure 1. CRISPR/Cas9 genome editing to generate INS-1 lines with 3.16 Mb deletions of the silent (maternal) and active (paternal) PWS-imprinted domain. (A) Gene map of the rat PWS-imprinted domain and CRISPR/Cas9-targeted deletions. Symbols: circles, protein-coding genes; thin ovals, RNA genes; blue, (paternal; pat) and red (maternal; mat), imprinted genes; IC, imprinting control region (purple bar); green boxes, CRISPR gRNA target sites; blue and red horizontal bars, extent of deletions. Not all copies of tandemly repeated loci (*miR-344*; U1, *Snord116*, *Snord115*) are shown. **(B)** Schematic showing generation of genome edited, clonal INS-1 lines with 3.16 Mb deletions on the silent maternal allele only (5-9, 2, 16; dark pink) or homozygous deletion of both maternal and active paternal alleles (3, 19-1, 19-4, 25; blue). **(C)** First round

deletion-PCR on genomic DNA identifies two INS-1 lines with deletions (5-9, 5-5). **(D)** DNA methylation analysis of bisulfite-modified genomic DNA at the PWS-IC establishes that lines 5-5 and 5-9 have deletions on the maternal allele. **(E)** Second round deletion-PCR identifies three INS-1 lines (3, 19, 25) with deletions on the paternal allele, with line 3 having an alternate proximal breakpoint. **(F)** Gene dosage of *Snord107* normalized to *Ube3a* as determined by ddPCR using genomic DNA from the INS-1 panel of cell lines (also see **Fig. S6**). **(G)** PWS-deletion lines (3, 19-1, 19-4) lack mRNA expression of the PWS-imprinted genes, *Snrpn* and *Snord116*, as detected by RT-PCR, whereas control lines (5-9, 2, 16) express PWS-imprinted genes. All cell lines express the control genes (*Gapdh*, *Ins2*). The full panel of PWS-imprinted genes is shown in **Fig. S7A,B**. **(H)** Use of whole cell extracts for a western blot shows that PWS-deletion lines (3, 19-1, 19-4) lack expression of the spliceosomal SmN polypeptide (24.6 kDa) encoded by *Snrpn*, but retain expression of the paralogous SmB polypeptide (23.6 kDa) encoded by the unlinked *Snrpb* gene. The control is α-Tubulin.

Figure 2:

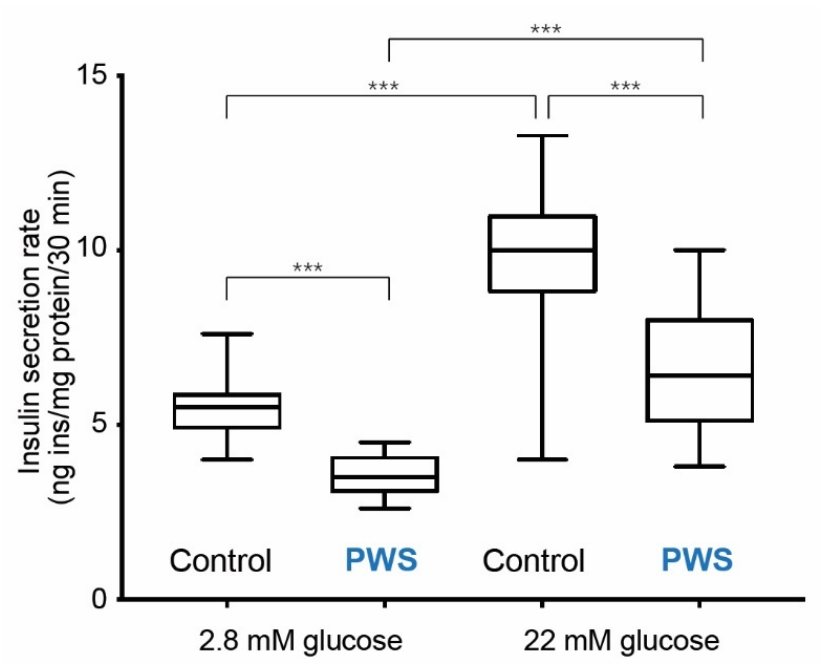

Figure 2. Deficient basal and glucose-stimulated insulin secretion in PWS-deletion INS-1 lines. PWS INS-1 cell lines have insulin secretion deficits at both low (2.8 mM) and high (22 mM) glucose, based on the pooled insulin secretory rates for each of PWS (3, 19-1, 19-4) and control (5-9, 2, 16) groups (n=36 biological replicates per group, with n=12 per cell line). Although glucose-stimulated secretion increased 1.75-fold for control and 1.85-fold for PWS, loss of the PWS genes decreased the secretory rate by 36% in basal 2.8 mM glucose conditions and by 32% in stimulatory 22 mM glucose conditions. Statistical comparison by ANOVA with Tukey post hoc test (***, $P < 0.0001$).

Figure 3:

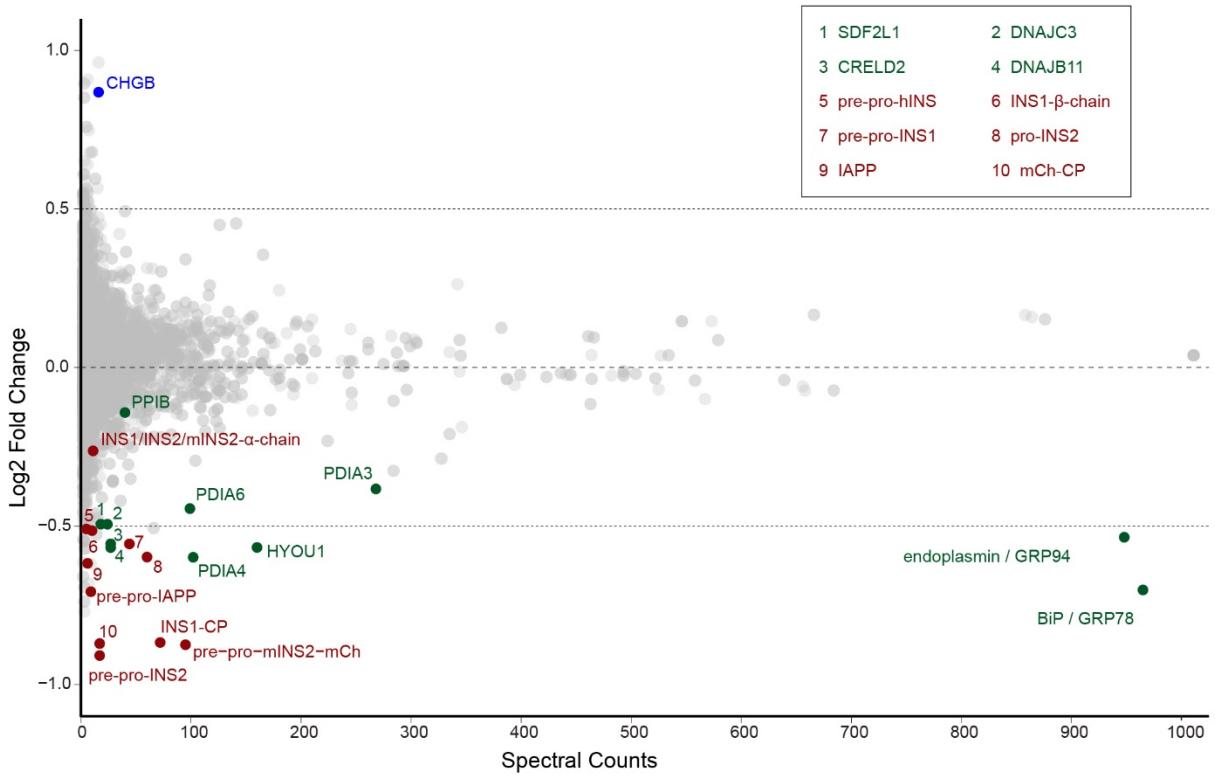

Figure 3. Proteome-wide alterations in PWS-deletion *vs.* control INS-1 lines identifies reductions in levels of ER chaperones and hormones. The 6-plex Tandem Mass Tag (TMT) system for quantitative proteomics was used to compare trypsin-digested proteins from cellular lysates following methanol-acetic acid extraction of PWS (3, 19-1, 19-4) *vs.* control (5-9, 2, 16) INS-1 β-cell lines. Cells were treated under insulin secretion conditions, 30 min in KRH buffer with high (22 mM) glucose. The vast majority of the proteins measured remained unchanged with a Log2 Fold Change (PWS/control ratio) near 0 as expected. Protein levels of 11 ER chaperones (green) as well as secreted hormones (red) insulin [various processed forms of INS1, INS2, mouse (m) mINS2-mCherry (mCh), human (h) INS, and C-peptide (CP); mature INS is the 21 amino acid peptide identical between rat INS1, rat INS2 and mouse INS2] and amylin (full length and

processed IAPP) were markedly reduced in PWS INS-1 cell lines. In contrast, chromogranin B (CHGB) levels are noticeably increased in PWS INS-1 cell lines (blue). The boxed Key indicates the identity of the 10 numbered peptide spots.

Figure 4:

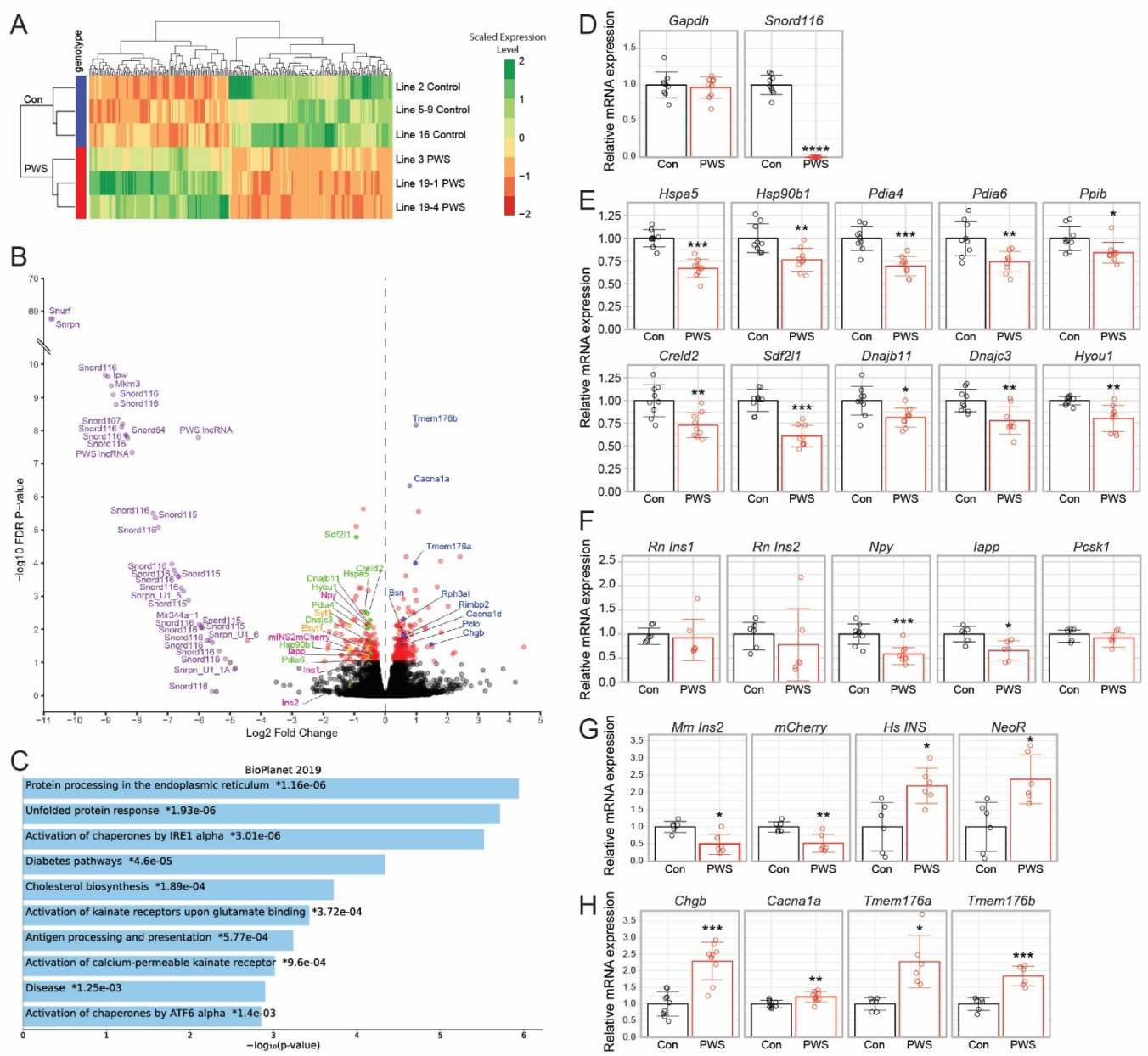

Figure 4. Genome-wide transcriptome alterations in PWS-deletion *vs.* control INS-1 lines identifies significant differentially expressed genes (DEGs) including those encoding endoplasmic reticulum (ER) chaperones and hormones. (A) Heatmap clustergram of 228 DEGs demonstrates tight clustering of PWS *vs.* control groups (*Padj* < 0.05). Scale: green (enriched) to red (depleted). RNA-seq was performed for 3 PWS (3,

19-1, 19-4) *vs.* 3 control (5-9, 2, 16) INS-1 cell lines. **(B)** Volcano plot showing statistical significance (-log10 FDR *P*-value) *vs.* magnitude of change (Log2 Fold Change) for all expressed genes. Colored data points indicate PWS-imprinted genes (purple), ER chaperones (green), secreted proteins (pink), synaptotagmins involved in insulin secretion (yellow), proteins involved in neuronal active zone/exocytosis and vesicle acidification (blue), and all other significant genes (red, without labels). **(C)** Gene set enrichment analysis identifies key biological pathways involved in protein processing and the unfolded stress response in the ER. **(D-H)** Relative gene expression of control (Con, black; 5-9, 2, 16) *vs.* PWS (red; 3, 19-1, 19-4) determined by RT-ddPCR normalized to *Gpi* levels and to the average expression in control INS-1 lines, including for **(D)** *Gapdh* and *Snord116* (PWS) control genes, **(E)** ten downregulated DEGs encoding ER chaperones, **(F)** endogenous *Rattus norvegicus* (Rn) genes encoding β-cell hormones and secretory proteins, **(G)** exogenous insulin transgenes in the INS-1 lines (*Mm*, *Mus musculus*; *Hs*, *Homo sapiens*) as well as mCherry and neomycin resistance (*Neo*R) marker proteins, and **(H)** upregulated DEGs involved in the secretory pathway. Statistical comparison by Welch's t-test: *, $P < 0.05$; **, $P < 0.005$; ***, $P < 0.0005$; ****, $P < 0.00005$.

Figure 5:

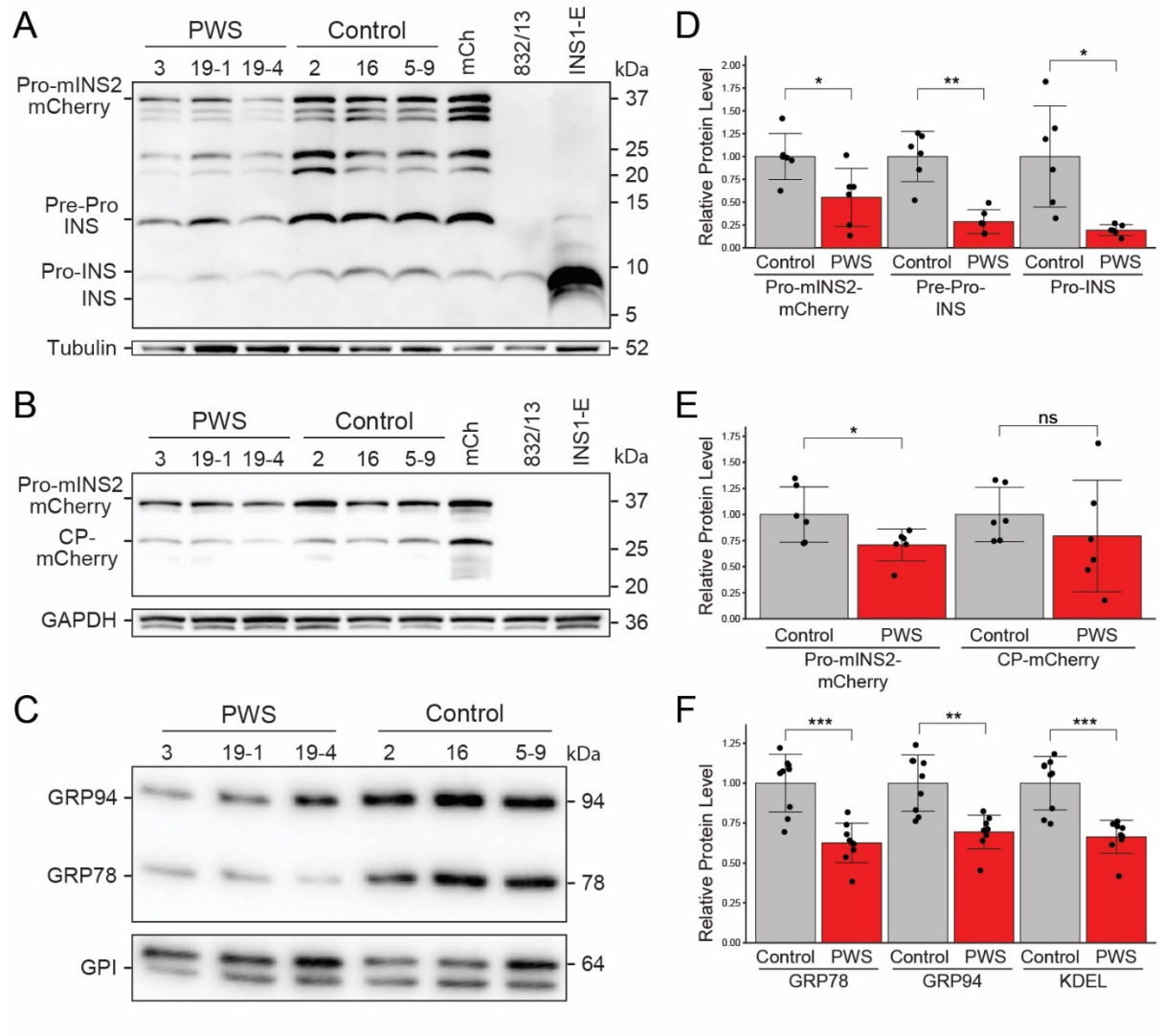

Figure 5. Reductions in insulins and ER chaperone levels in PWS-deletion *vs.* control INS-1 lines. (A-C) Western blots of whole cell lysates from PWS (3, 19-1, 19-4) and control (5-9, 2, 16) INS-1 β-cell lines grown under control (DMSO) conditions for 5 h were assessed using a panel of antibodies. **(A)** Anti-insulin, detecting all cellular forms of insulin (Pre-Pro-, Pro-, and fully processed rat INS) as well as mouse proinsulin2 (Pro-mINS2)-mCherry. **(B)** Anti-mCherry, detecting mouse proinsulin2 (Pro-mINS2)-mCherry and C-peptide (CP)-mCherry. **(C)** Anti-KDEL, detecting the two major ER chaperones

GRP94 (endoplasmin; HSP90B1) and GRP78 (BiP; HSPA5). Anti-α-Tubulin, anti-GAPDH, and anti-GPI were used as controls for protein loading levels in **(A)**, **(B)**, and **(C)**, respectively. For **(A)** and **(B)**, control cell lines included INS-1::mCherry (mCh), INS-1 832/13 parental, and INS1-E. **(D)** Quantitation of Pro-mINS2-mCherry, Pre-Pro-INS and Pro-INS detected with anti-insulin in the PWS and control INS-1 lines (n=6 each genotype). **(E)** Quantitation of Pro-mINS2-mCherry and CP-mCherry detected with anti-mCherry in the PWS and control INS-1 lines (n=6 each). **(F)** Quantitation of GRP78, GRP94, and total KDEL detected with anti-KDEL in the PWS and control INS-1 lines (n=9 each). For **(D-F)**, statistical comparison by Welch's t-test: *, $P < 0.05$; **, $P < 0.005$; ***, $P < 0.0005$; ns, not significant.

Figure 6:

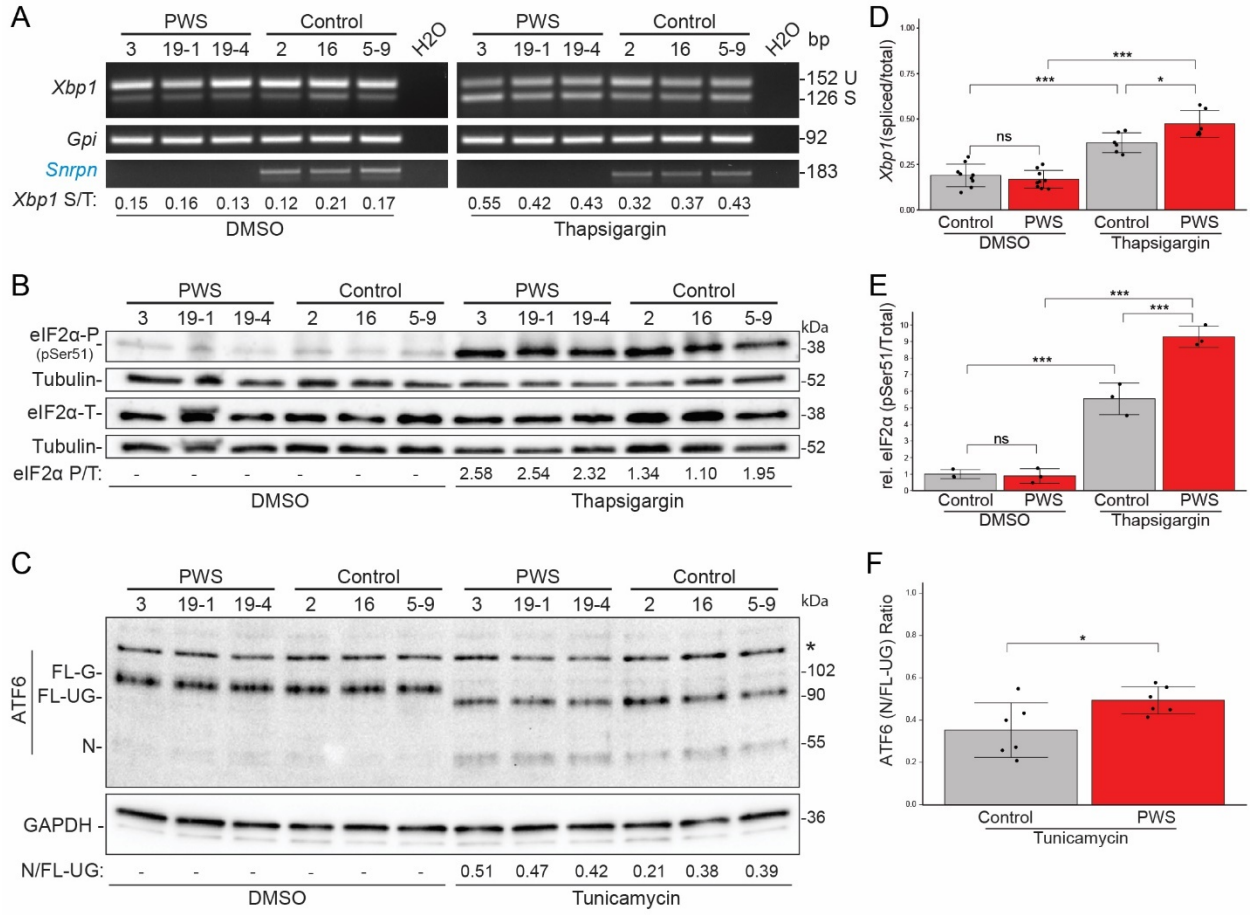

Figure 6. More sensitive activation of all three ER stress master regulatory pathways in PWS-deletion *vs.* control INS-1 β-cell lines. (A) For the IRE1α pathway, we assessed its mRNA processing of *Xbp1* from unspliced (U) to spliced (S), with control gene *Gpi* and PWS-*Snord116* also assayed by RT-PCR, using RNA from PWS (3, 19-1, 19-4) and control (5-9, 2, 16) INS-1 cell lines treated with DMSO or 0.1 μM thapsigargin for 3 h. At bottom, the *Xbp1* S/T (spliced/total) ratios for each cell line are shown, under both control (DMSO) and ER stress (thapsigargin) conditions. **(B)** The PERK pathway was assessed by comparison of total eIF2α to PERK phosphorylated eIF2α-P (pSer51), using whole cell lysates from PWS and control INS-1 cell lines treated with DMSO or 0.1 μM thapsigargin for 5 h. Anti-αTUB was used as a control for protein-loading levels. At

bottom, the eIF2α P/T (phosphorylated/total) ratios for each cell line are shown under the ER stress (thapsigargin) condition. **(C)** For the ATF6 pathway, we used whole cell lysates from PWS and control INS-1 cell lines treated with DMSO or 10 μg/ml tunicamycin for 5 h. Under control DMSO conditions, full-length (FL) and glycosylated (G) ATF6 of ~ 100-kD is ER-localized. tunicamycin inhibits biosynthesis of N-linked glycans, resulting in unglycosylated (UG) ATF6-FL of 90-kD in the ER, with proteolytic processing in the Golgi to produce nuclear (N) ATF6-N of ~55-kD. *, non-specific band detected by the anti-ATF6 antibody. Anti-GAPDH was used as a control for protein-loading levels. At bottom, the ATF6 N/FL-UG (nuclear/FL-unglycosylated) ratios for each cell line are shown under the ER stress (tunicamycin) condition. **(D)** Quantitation of the ratio of spliced/total (S/T) *Xbp1* mRNA in the PWS and control INS-1 lines under control (DMSO; n=9 each genotype) and thapsigargin (3 h; n=6 each) conditions. PWS β-cells are more sensitive to thapsigargin-induced ER stress with earlier and more robust activation of *Xbp1* mRNA splicing than control cell lines. **(E)** Quantitation of the relative (rel.) level of phosphorylated (pSer51) to total eIF2α in the PWS and control INS-1 lines (n=3 each) under control (DMSO) and thapsigargin conditions. PWS cells are more sensitive to thapsigargin-induced ER stress with more robust activation of eIF2α phosphorylation. **(F)** Quantitation of the ratio of nuclear/FL-unglycosylated (N/UG) for ATF6 in the PWS and control INS-1 lines under ER stress (tunicamycin) conditions (n=6 each, from two biological replicates). PWS cells are more sensitive to tunicamycin-induced ER stress with more robust activation of ATF6-N. For **(D-E)**, statistical comparison by ANOVA and for **(F)** by Welch's t-test with Tukey's HSD post-hoc: *, $P < 0.05$; **, $P < 0.005$; ***, $P < 0.0005$; ns, not significant.